Stony Brook University

Novel adhesive properties of poly(ethylene-oxide) adsorbed nanolayers

A Thesis Presented

by

Wenduo Zeng

to

The Graduate School

in Partial Fulfillment of the

Requirements

for the Degree of

Master of Science

in

Materials Science and Engineering

Stony Brook University

May 2015

Stony Brook University

The Graduate School

Wenduo Zeng

We, the thesis committee for the above candidate for the

Master of Science degree, hereby recommend

acceptance of this thesis.

Tadanori Koga – Thesis Advisor
Associate Professor, Department of Materials Science and Engineering

Jonathan Sokolov– Second Reader

Professor, Department of Materials Science and Engineering

T. Venkatesh – Third Reader

Associate Professor, Department of Materials Science and Engineering

This thesis is accepted by the Graduate School

Charles Taber
Dean of the Graduate School

Abstract of the Thesis

Novel adhesive properties of poly(ethylene-oxide) adsorbed nanolayers

by

Wenduo Zeng

Master of Science

in

Materials Science and Engineering

Stony Brook University

2015

Abstract

Solid-polymer interfaces play crucial roles in the multidisciplinary field of nanotechnology and are the confluence of physics, chemistry, biology, and engineering. There is now growing evidence that polymer chains irreversibly adsorb even onto weakly attractive solid surfaces, forming a nanometer-thick adsorbed polymer layer ("adsorbed polymer nanolayers"). It has also been reported that the adsorbed layers greatly impact on local structures and properties of supported polymer thin films. In this thesis, I aim to clarify adhesive and tribological properties of adsorbed poly(ethylene-oxide) (PEO) nanolayers onto silicon (Si) substrates, which remain unsolved so far. The adsorbed nanolayers were prepared by the established protocol: one has to equilibrate the melt or dense solution against a solid surface; the unadsorbed chains can be then removed by a good solvent, while the adsorbed chains are assumed to maintain the same conformation due to the irreversible freezing through many physical solid-segment contacts. I firstly characterized the formation process and the surface/film structures of the adsorbed nanolayers by using X-ray

reflectivity, grazing incidence X-ray diffraction, and atomic force microscopy. Secondly, to compare the surface energy of the adsorbed layers with the bulk, static contact angle measurements with two liquids (water and glycerol) were carried out using a optical contact angle meter equipped with a video camera. Thirdly, I designed and constructed a custom-built adhesion-testing device to quantify the adhesive property. The experimental results provide new insight into the microscopic structure - macroscopic property relationship at the solid-polymer interface.

Table of Contents

List of Figures

List of Tables

List of Schemes

List of Abbreviations

PEO: poly(ethelene-oxide)

AFM: Atomic Force Microscopy

GID: Grazing Incidence X-ray Diffraction

XR: X-ray Reflectivity

Acknowledgments

Firstly, I would like to express my deepest appreciation to my thesis advisor, Tadanori Koga, for his unending mentorship and guidance, helping me to hone and enhance my skills as a master's student. His sagacity as my teacher helped make this research and thesis possible. Throughout my research in the lab, he has imbued me with tremendous knowledge and understanding of polymer science which I will be sure to carry with me in my future endeavors.

My thanks also goes out to Naisheng Jiang, Mani Kuntal Sen, Deborah Barkley, Xiaoyu Di, Jiaxun Wang, Justin Cheung, all lab mates in Professor Koga's lab, who supported and helped me copiously during my time as a master's student.

A heartfelt thanks to my parents, Ke Wang and Funian Zeng, for their inexorable patience and gracious support of my master's studies as well as their infinite consideration of my wellbeing at Stony Brook University.

Chapter 1

1.1 Adhesion between polymer thin films

Adhesion is an intriguing complex procedure with regard to the interfacial region in a pair of two pieces of polymeric materials and the subsequent adhesive attraction. In many industrial fields and corresponding application methods, the issue of adhesion has been paid a growing attention. Although many experimental and theoretical studies have been conducted for the last few decades, the mechanism of adhesion and the structure-property relationship still remains uncleared.[2]

The interface between two films should endure a specific amount of force pulled vertically, which induces normal tension or friction in a horizontal direction, which induces shear stress or united group, to complete such characterization test for adhesive property. Adhesion can be divided into three categories: basic adhesion, thermodynamic adhesion, and practical adhesion.[3]

Basic adhesion is closely linked to the intrinsic property and extrinsic mechanical performance of the interaction between two materials. The origin of adhesive forces can also divide into three categories: (i) ionic, metallic and covalent could considered as primary valence type; (ii) H-bonding could be considered as "nearly" valence type due to its uniqueness; (iii) Van der Waals forces. However, this definition has been mainly demonstrated by theoretical calculations with few practical linkage or meaning. Thus this method is usually utilized for computational and simulation in related experimental research work.

The definition of thermodynamic adhesion is actual work that should be done to create an interface from two originally separate surfaces, which is thermodynamically reversible, as indicated by the following equation:

$$W_{AB}=\sigma_A+\sigma_B-\sigma_{AB} \quad (1):$$

where W_{AB} is the corresponding work of adhesion, σ_{AB} is the surface free energy of newly created interface, the other two parameters represent the original surface free energy of the two materials. In actual research practice, the interfacial free energy is always unknown parameters, hence the real procedure is to gain the value of $W_{AB,}$ σ_A and σ_B, and the value of σ_{AB} can be gained. The

third category of adhesion is defined as experimental adhesion. Practically, this part of research can be characterized by two factors: (1) the stress that is the critical force per unit area to break up two attached substances; (2) the critical workload that could make the separation completely.

In this research I consider the adhesion between two thin films. Also, my attention is limitedly to adhesion associated with polymer chain motions and entanglements instead of chain linkage and bonds through chemical reaction, or "hitch" from a mechanical perspective because of irregularity and coarseness of surfaces.

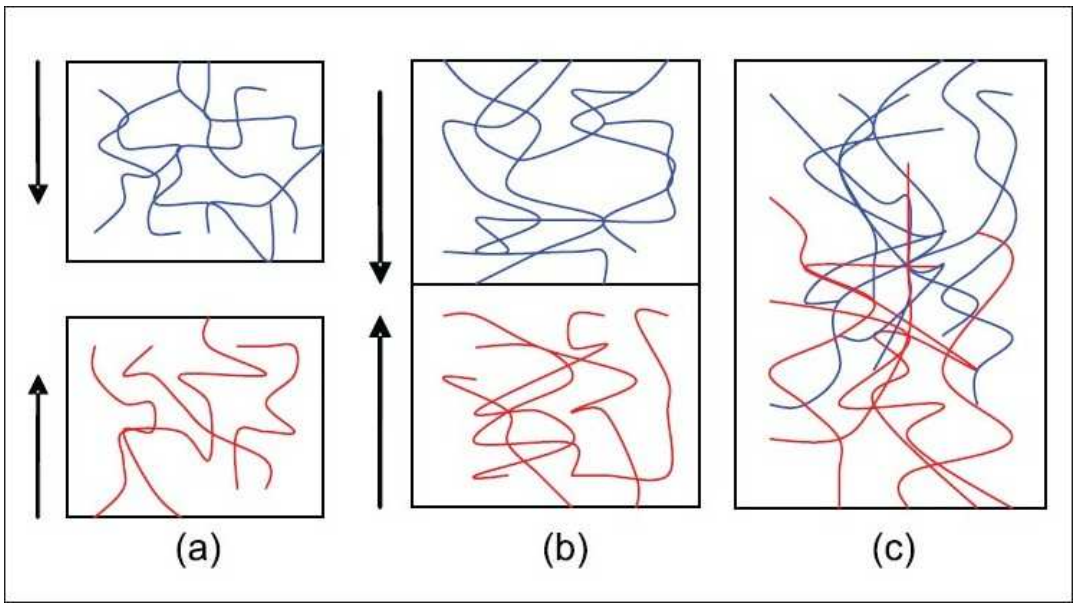

Figure 1. The schematic image showing the adhesion between polymer thin films due to chain motion into each other. (a), (b) and (c) represent the different stages of two pieces of polymer having contact with each other and polymer chain interdiffusing.[4]

1.2 Adhesion between polymers correlated with interfacial entanglements

Most pairs of common polymers have quite considerable enthalpy of mixing so that phase separation typically occurs as a result of mixing or blending. Hence, it is expected that the interfacial strength between two polymers is not so strong.

The magnitude of unit for theoretical computation of the adhesive strength when it comes to different kinds of polymeric material are always used as mJ/m^2, while in actual measurement it is

more reasonable to choose the unit of J/m^2. This conspicuous contrast demonstrates that the importance of chain entanglement of affording excessive adhesion strength except for other factors.

During melting process when pressing two pieces of polymers together, a zone of two polymer films overlapping with each other will form although it is not broad. In contrast to the region with clearly denoted boundary, the interfacial region between two polymer thin films is actually a transient region. That is to say, the density of one kind of polymer chain will show increasing gradient in one direction within this region while the chains of another polymer will decrease in such direction. As entanglements are becoming stable at their positions due to exterior environment changes such as evaporation of solvent or cooled from its "flexible" state, polymeric materials with contact points could attach to each other, since there are so many physical links between them to keep them fixed. The interfacial width, as an important factor and parameter in controlling this whole research, with regard to different aims, plays a significant role of manipulating the amount of sites for chains where entanglements could take place. This parameter is strongly dependent on the corresponding experimental temperature, pressure, time and chemical properties of utilized polymers.

As for most polymeric systems, the polymer chain entanglements can be considered as the major source for them to get attached with each other, fracture mechanisms are divided into three categories: (1) scission; (2) pullout; (3) crazing. Fig.2 shows the molecular weight dependence of the corresponding mechanism.[5]

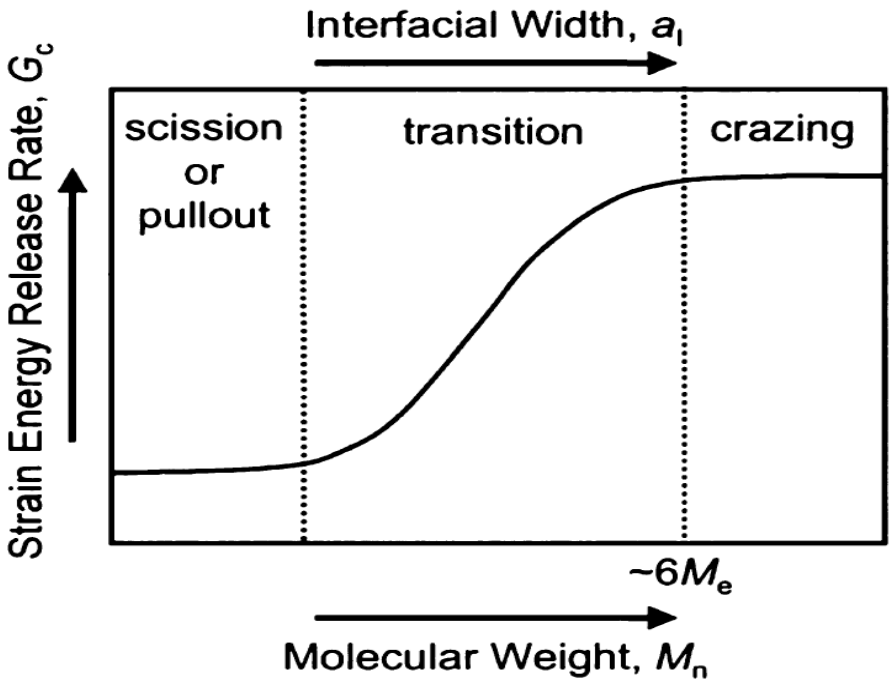

Figure 2. Illustrative increase of strain energy release rate, which is closely related to fracture and adhesive property, with molecular weight dependence.[5]

When we consider breaking up two immiscible polymeric systems, the horizontal axis can be changed into interfacial width to better characterize the whole process of elastic deformation to plastic deformation, and yielding and finally fracture.

In Fig. 3, a complete chain scission procedure of the two different polymeric system is shown. As discussed above, in contrast to other material systems such as metal or ceramic, a polymeric system usually possesses much weaker adhesive strength in the region of crazing so that the chain scission would have more common applications in actual research analysis. As shown schematically, every chain entanglement should be broken up in the interfacial region in order to keep the crack moving. Microscopically, the total forces to separate two pieces of material is the sum of shearing every entanglements.[6] And the dark region in the right middle part is the entire workload to create two new surfaces by integrating forces and displacement.[7]

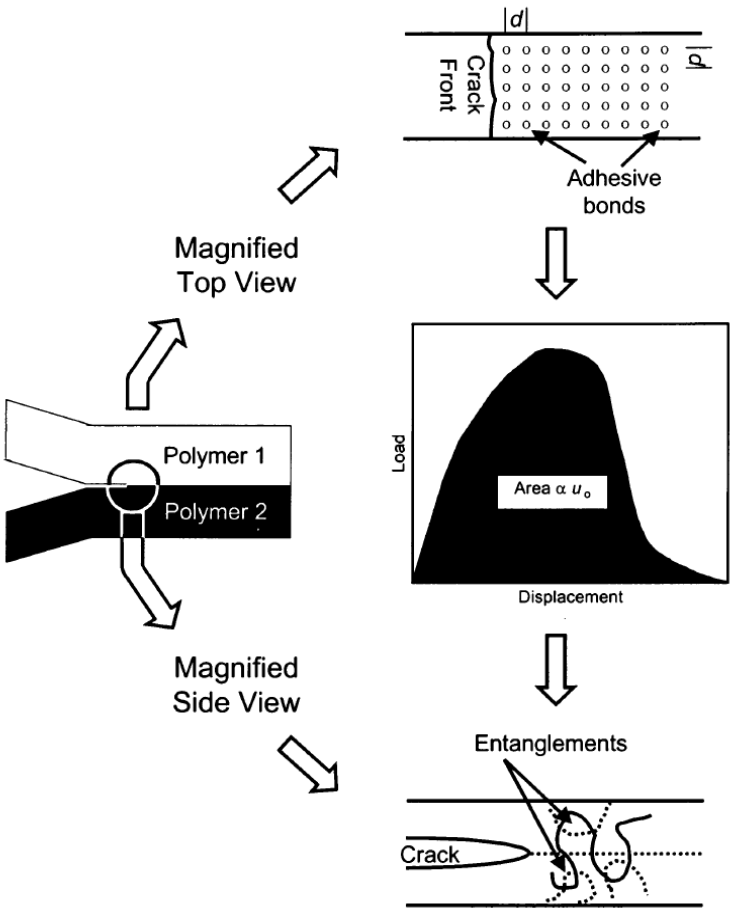

Figure 3. Illustrative image of two different polymeric system undergoing a chain scission procedure. [6,8]

1.3 Effects of contact angle and surface tension on adhesion

A consideration of such a model by shearing chain entanglements to advocate separation between attached substances is an opinion from a microscopic point of view. On the other hand, when the research major concern goes to macroscopic field, that is to say, diverse surface free energy of different material becomes an emphasis macroscopically or thermodynamically. To ensure a theoretically thermodynamic balance instead of molecule deformation and transformation discussed before, the whole system will make an overture to adjust itself aiming to get the minimization of surface free energy to lower reaction enthalpy or activation energy barrier as much as possible.

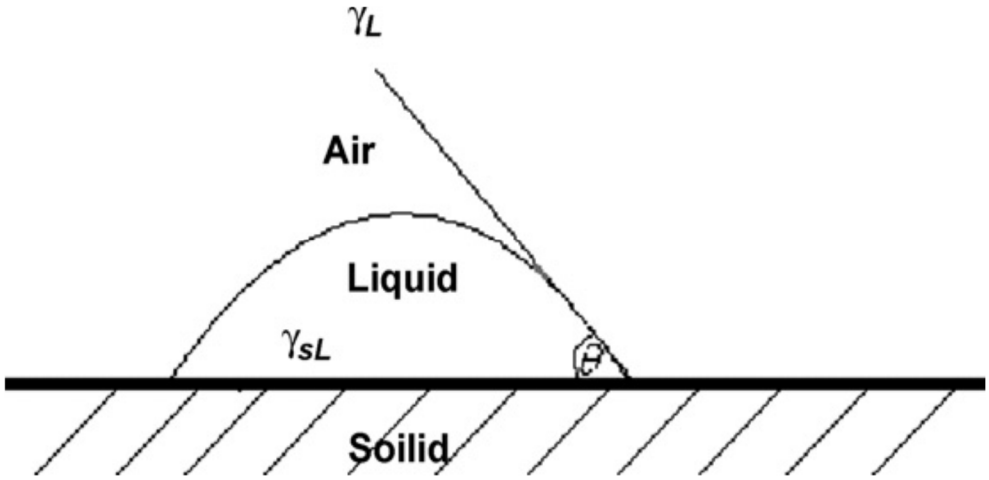

Figure 4. Droplet on impenetrable surface showing relevant parameters and their correlated relationship.[9]

Young propose his significant discovery in 1855 showing the interactive relationship between the droplet of a test liquid, the impenetrable solid and the neutrally exterior environment such as air (reference). Note that the surface here is isostructural, smooth and without morphological coarseness or reactive sites. The popular viewpoint of research to overcoming the inaccuracy due to the heterogeneity or hysteresis is by utilizing dynamic contact angle measurement.

$$\sigma_s = \sigma_l * \cos\theta + \sigma_{sl} \quad (2)$$

With the concept and definition discussed above, the work of adhesion can be calculated, which could refer to the thermodynamical adhesion. The main obstacle of applying for this method is that researchers could only get the exact value of the surface tension of the test liquid, while the counterpart for this solid should be evaluated by applying for Young`s equation and utilizing several combinations of different test liquids.

1.4 Polymer adsorbed nanolayer formation and its structure

For polymer samples fabrication and relevant manipulation of its microstructure, heat treatment is an essential part in the whole research procedure. In the solid-polymer melt (SPM) interface, the effect of thermal annealing helps polymer chain physically adsorb onto a impenetrable solid, a silicon substrate in our case. The adsorption procedure starts with lone chains aligned densely and uniformly with chain orientation being parallel to solid and the thickness of ~ 2 nm regardless of

its molecular weight and relevant to its own intrinsic property.[10] At the same time, a new late arriving polymer chains can adsorb onto the Si substrate. But for them a space is limited such that the later arriving chains need to attach to empty sites on substrate[11] From our previous research, the results indicate that by controlling the diverse parameters in actual heat treatment and following solvent leaching procedure, the two layers of poly(ethelene-oxide) with different structure and morphological properties could be uncovered. By utilizing chlorobenzene, we could directly extract the lone flattened layer with higher density, while both loosely adsorbed chains and flattened chains (we hereafter assign this an "interfacial sublayer") can be extracted with toluene, which is a relatively poor solvent compared to chlorobenzene. Fig. 5 shows the schematic view of the two different chain conformations of the adsorbed chains on the solid.

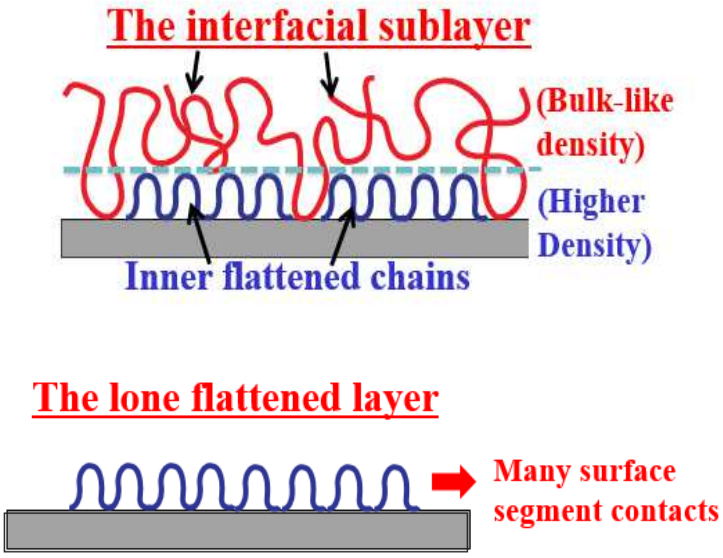

Figure 5. The sketch image showing the different chain structure of two adsorbed nanolayers.

In order to inquiry the crystal structure and surface morphology, the corresponding characterization is done. Like the AFM images and GID pattern shown in fig. 6 and 7, it is indicating that the 8.5nm adsorbed nanolayer, i.e. interfacial sublayer, shows a crystallization behavior along (120) orientation while the 2.5nm adsorbed nanolayer, i.e. inner flattened layer, shows no crystallization at all and remain homogeneous.[12]

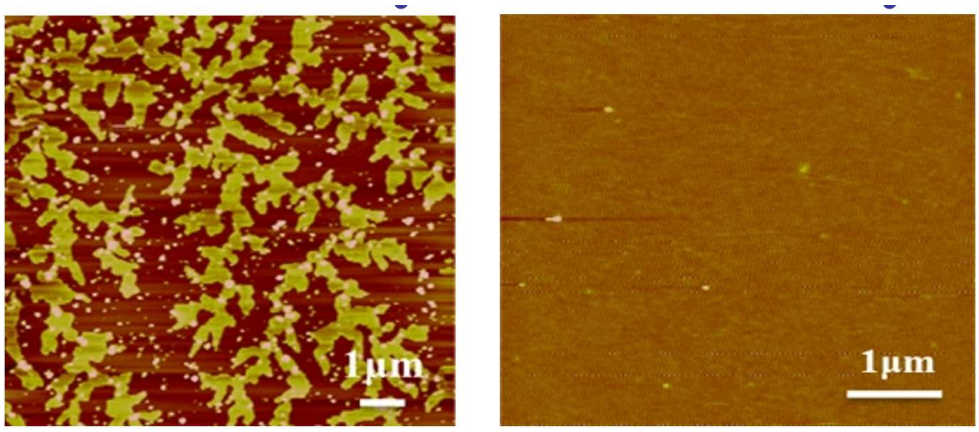

Figure 6. The AFM image showing surface morphology (left is interfacial sublayer and right is inner flattened layer).

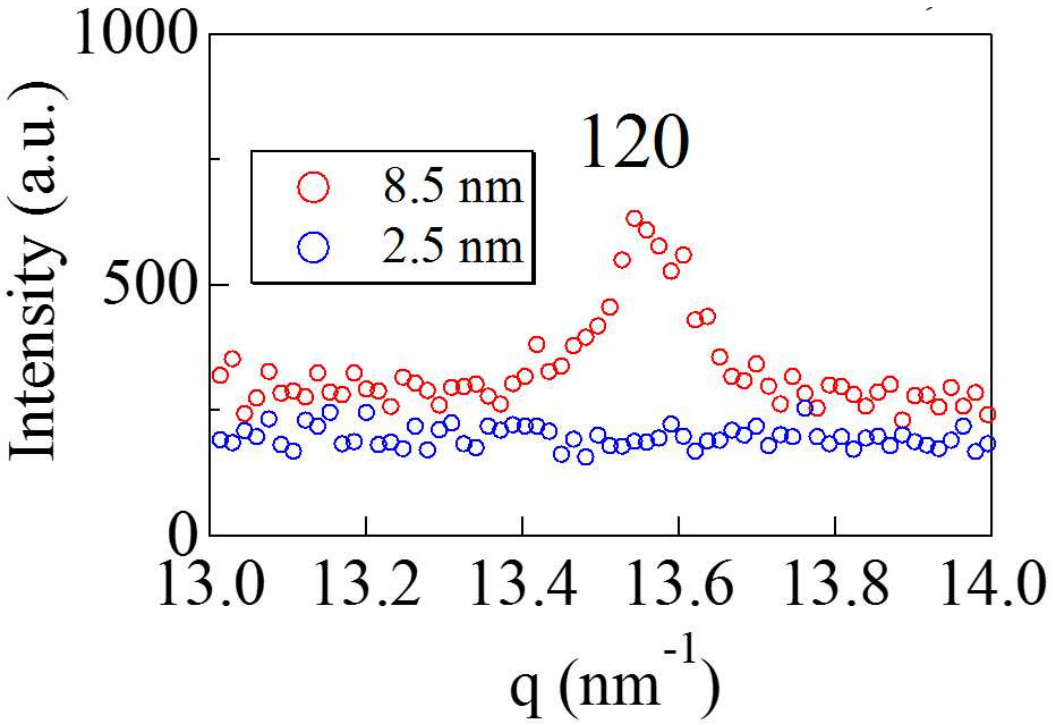

Figure 7. GID pattern characterizing the structure difference between interfacial sublayer and flattened layer.

1.5 Dewetting behavior at the adsorbed polymer-free polymer interface

The behavior of a fluid thin film that collapses on an impenetrable planar solid is so-called "dewetting". And usual consequence of this phenomenon causes formation of a droplet.

Macroscopically, the whole process can be considered as the counterpart of wetting. Such a physical transformation is significantly important for many industrial fields and device utility, and the most essential one is adhesion. In most cases, this phenomenon is unwanted because it hugely deteriorate the wholly completeness of applicative material systems due to a series of interfacial issues including mechanical and physical instability.[13]

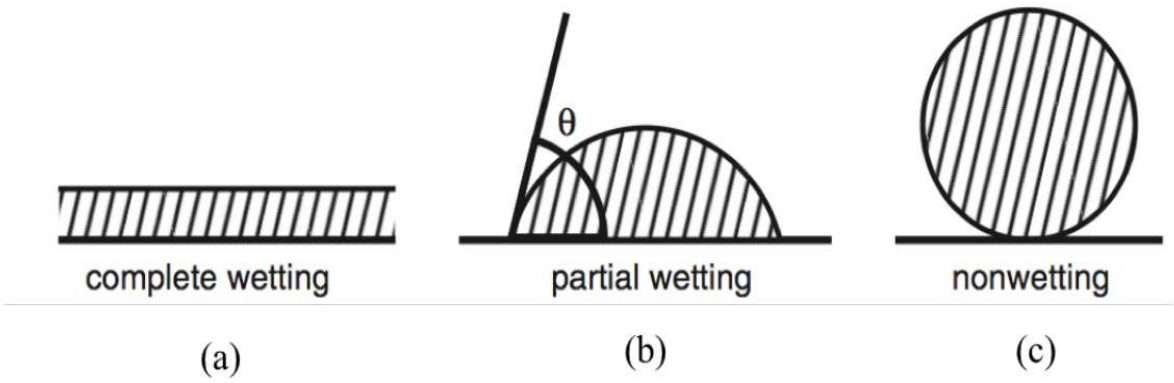

Figure 8. The illustrative image showing complete wetting, partial wetting and notwetting, separately.

As shown in Fig. 8, once dewetting occurs, the upper film endures a rupture or deformation to form into a new droplet which leaves quite large area uncovered. From a macroscopic view, this is adhesion failure or fracture between two attached substances, especially thin films in this case. The main reason for this behavior is closely correlated to the interaction between the two layers. If the interaction is too weak to offset the incompatibility between these two pieces, the upper thin film is then to undergo a dewetting. We here discuss the interaction mainly associated with physical bonds induced polymer chain motions and thus entanglements.

Chapter 2

2.1 Sample Preparation

Four different poly (ethelyne-oxide) (PEO) (1. average M_w=1.5kDa, Fluka Analytical, product no. 81210, 2. average M_w=8kDa, Sigma-Aldrich, product no. 202452, 3. average M_n=20kDa, Sigma-Aldrich, product no. 81300, 4. average M_v=100kDa, Sigma-Aldrich, product no. 181986) were used to study the corresponding mechanical and adhesive properties. Si substrates cleaned with the so-called "piranha solution" were used as substrates. The piranha solution is a mixture of highly corrosive H_2O_2 and H_2SO_4, which needs extremely careful treatment of handling and prevention from physical contact with human body. After this washing process, the substrate was washed with DI water for several times in order to fully erase the residual liquid used. Finally, these substrates were dipped into a 5% HF aqueous solution to remove a native oxide layer (SiO_2) for 15-30 seconds. From X-ray reflectivity characterization, we confirmed that the thickness of the SiO_2 layer was 1.3 nm (this reconstruction of the SiO_2 layer is due to oxygen in air), while the thickness of the SiO_2 layer without the HF treatment was estimated to be 2.4 nm. PEO thin films of different thickness were prepared from several polymer/toluene solutions by utilizing spin coating. The rotation time was fixed to 30 seconds and the rotation speed was 2500 rpm. With the refractive index of 1.455 for PEO, the thickness was characterized by utilizing ellipsometry (Rudolf Auto EL- II). We used the HF-passivated silicon substrate for this study due to more attractively interactive system with PEO.

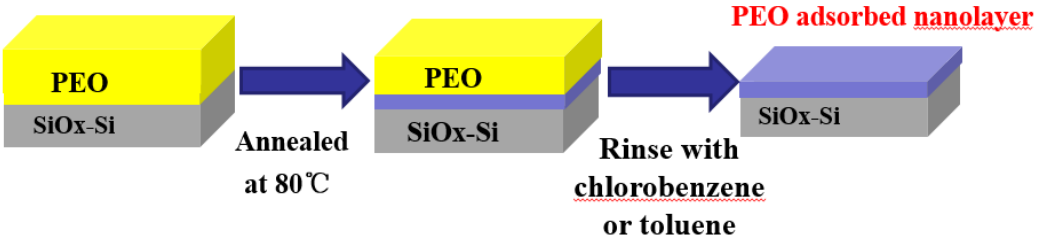

Scheme 1. Sample preparation process used in experiment

2.2 Custom-built adhesion testing device

The fracture strength between two polymer layers were characterized by a custom-built adhesion testing device based on the principle of Hook`s Law.[14] A mechanical spring, which has a spring constant of 400N/m, was used.[14-16]

After the polymer adsorbed layers (i.e., the flattened layers and the interfacial sublayers) along with thin films as controls were prepared on the H-Si substrates, the respective film was pressed together with a PEO thin film of 200nm prepared on the H-Si, resulting in a bilayer. The bottom adsorbed layer prepared on the H-Si was fixed to an experimental stage, while the upper bulk sample is being attached to one end of the mechanical spring.[16] Once the other end of the spring is being pulled and the force, which exceeds the maximum that the two attached sample could endure, was recorded as the critical fracture force. At the same time, the displacement of the spring was monitored and documented. The fracture force was simply calculated by using the spring constant multiplied by displacement. And the surface area of the samples were fixed to 1cm*1cm, thus the fracture stress can be calculated as the fracture force divided by the surface area.[17]

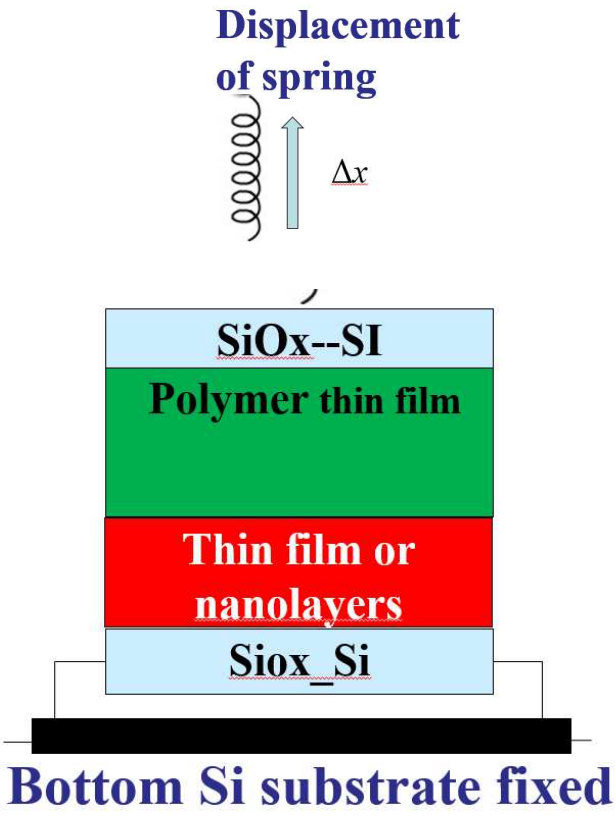

Scheme 2. Device setup and experiment procedure.

2.3. X-ray Reflectivity (XR) measurements

The adsorbed nanolayers were characterized by XR experiments at the X20A beamline, National Synchrotron Light Source, Brookhaven National Lab. Reflectivity was measured as a function of scattering vector normal to the film surface, $q_z = (4\pi\sin\theta)/\lambda$, θ is the incident angle and λ is the wavelength of X-ray (0.118 nm in this experiment). The specific data fitting procedure will be briefly discussed in the next chapter.

2.4. Atomic Force Microscope (AFM) measurements

Surface morphology of the PEO thin films was studied by atomic force microscope (AFM) (Digital Nanoscope III). A standard tapping mode was conducted in air using a cantilever with a

spring constant of ~ 40 N/m and a resonant frequency of ~300 kHz. The scan rate was 1.0 Hz with the scanning density of 256 or 512 lines per frame.

2.5 Grazing incidence X-ray diffraction (GID) measurements

Grazing incidence X-ray diffraction (GID) measurements for the interfacial sublayer as well as a spin cast PEO thin film were carried out at the X22B beamline at the National Synchrotron Light Source (NSLS), Brookhaven National Laboratory (BNL). Two dimensional diffraction patterns were measured with a CCD camera (Princeton Instruments) with an incident X-ray angle of 0.2°, which is above the critical angle of PEO, hence the films could be illuminated entirely. The X-ray wavelength was 0.15 nm and the exposure time for all the measurements was 400s.

Chapter 3 Result and discussion

3.1 Adsorption kinetics of PEO inner flattened layer

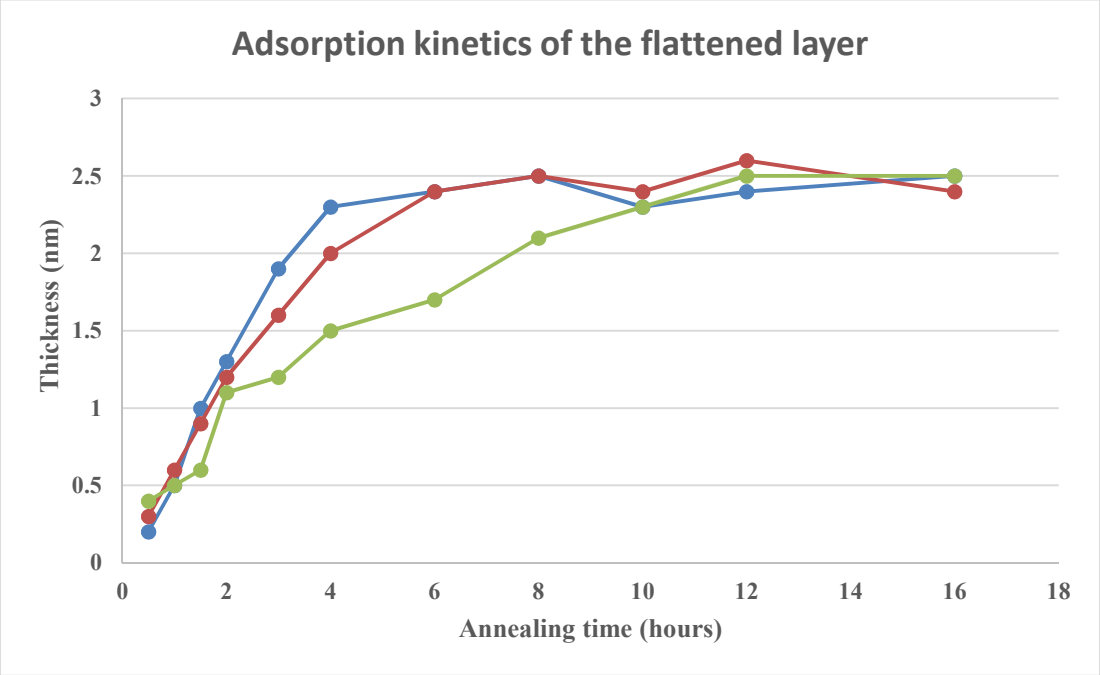

Figure 9. Growth of the flattened layer of PEO with molecular weights of 8kDa (blue dots), 20kDa (red dots) and 100kDa (green dots) against annealing time at 80℃.

Fig. 9 shows the thickness of the PEO flattened layer measured by ellipsometry against annealing time. The PEO flattened layer exhibits rapid growth at the initial stage of the process and there is a different equilibration time to reach the saturated regime for each sample. The equilibration times are 4 h, 6 h, 11 h for 8kDa, 20kDa and 100kDa. Hence, the experimental finding that the final thickness of the PEO flattened layer (~2.4 nm) for all three different molecular weights remained unchanged is consistent with our previous discovery.[12]

3.2 X-ray reflectivity characterization

Fig. 10 shows the XRR data for 20kDa PEO flattened layer at room temperature. To fit the data, we used a three-layer model (Si, SiO_2 and PEO flattened layer).

Scheme 3. Illustrative image of a 3-layer model

The fitting process of the acquired data point was done manually. By continuously adjusting three parameters (thickness, roughness, and dispersion value that is proportional to the density of a layer), the fitting was optimized. Fig. 10 shows the best fitting result. From the results, we can see that the dispersion value is (2.76±0.04) $\times 10^{-6}$, which is slight higher than the bulk by 7.5%. The best-fit also gives the thickness of 23.8±0.5Å, which is consistent with ellipsometry result.

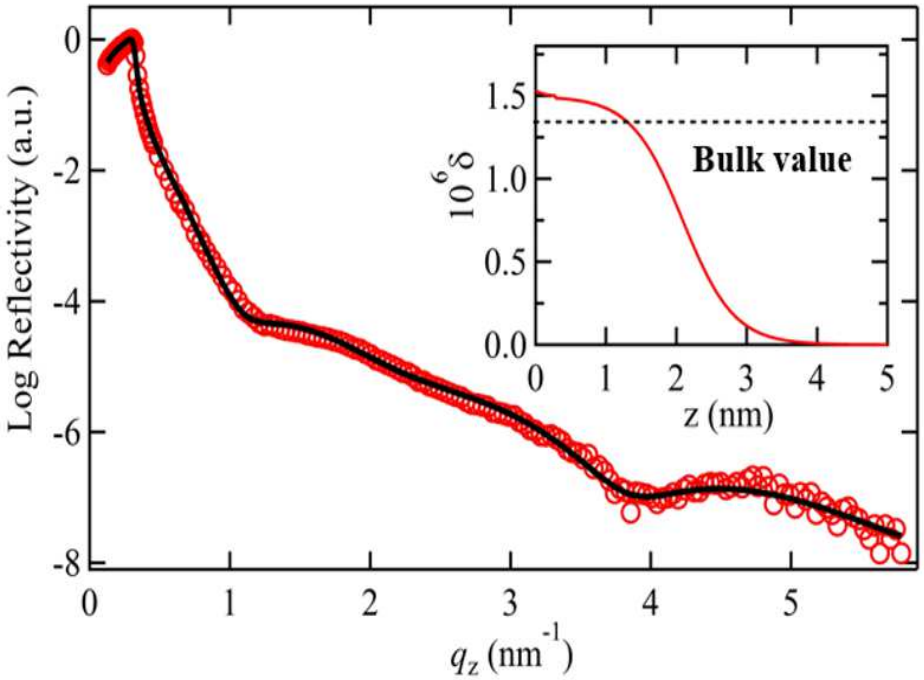

Figure 10. XRR data of 20kDa PEO flattened layer at room temperature.

3.3 High temperature GID characterization for determination of the melting point

In this section, I also characterized the crystal structure of the PEO interfacial sublayer along with a spin cast thin films. GID can be used as a method to quantify surface crystalline structures of the films.

Fig. 11 displays the two dimensional GID patterns of the PEO spin cast thin film and its interfacial sublayer at different temperatures. We fixed the annealing temperature and crystallization temperature to 80°C and 25°C, respectively.

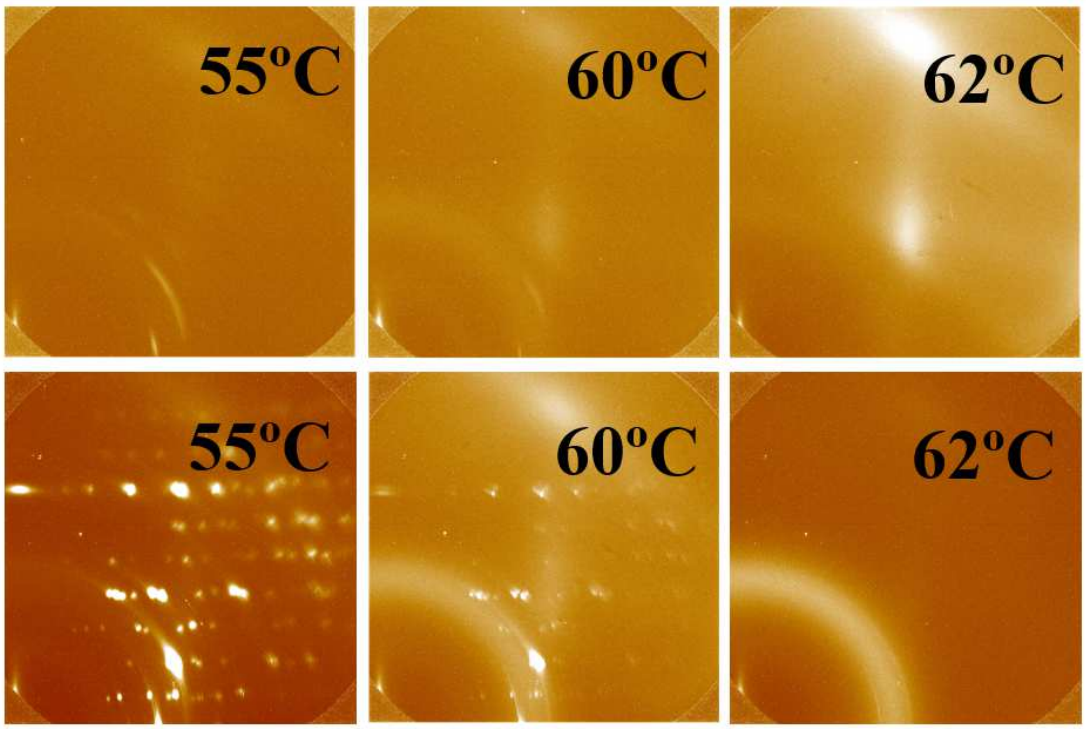

Figure 11. Two dimensional GID pattern of PEO spin cast thin film and interfacial sublayer with experimental temperature indicated at the upper right corner for each individual image (The upper row shows interfacial sublayer, while the lower row shows the spin cast thin film)

Obviously, with increasing temperature, the crystallized structure is gradually melted: diffraction peaks in the GID patterns for either spin cast thin film or the interfacial sublayer become

less discrete. From the data, it is reasonable to conclude that the melting point of the interfacial sublayer is bulk-like.

3.4 Fabricating groups of two polymer layers

We utilized several pairs of bilayers for the adhesion experiments, as tabulated in Table 1 for M_w=8kDa and the same pairs of bilayers were prepared for 20kDa and 100kDa.

Table 1. The combination of samples of molecular weight of 8kDa.

Upper layer	**200nm thin film**								
Bottom layer	**(1) Inner flatten layer**	**(2) 2.5nm thin film**	**(3) Inter-facial sublayer**	**(4) 5nm thin film**	**(5) 8.5nm thin film**	**(6) 15nm thin film**	**(7) 50nm thin film**	**(8) 100nm thin film**	**(9) 200nm thin film**

As indicated in the table, the thickness of the upper layer was fixed to 200nm, while the thickness of the bottom samples was varied from 2.5 nm to 200 nm. Besides, the flattened layer and interfacial sublayer were prepared to illuminate the effect of the different chain confirmations on the adhesion force. Note that the thickness of the interfacial sublayer depends on the molecular weight: 15 nm for M_v=100kDa, 8.5nm for M_n=20kDa, and 5 nm for M_w=8kDa.

3.5 Optimization of experimental parameters

In order to make sure that the adhesive strength between the two polymer layers has reached in equilibrium, two optimized experiments were performed with varying adhesion temperatures and pressing times. As shown in Figs. 12 and 13, the temperature and time dependence of the fracture strength for PEO (M_n=20kDa) were characterized.[18]

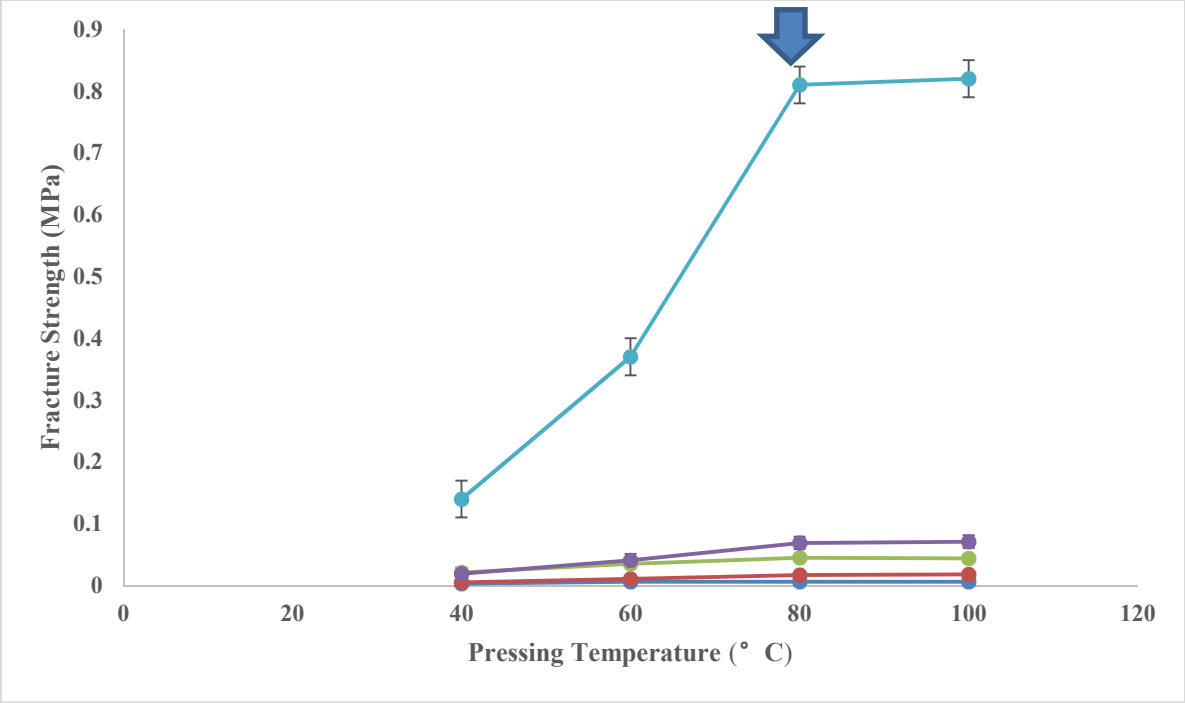

Figure 12. Temperature dependence of the fracture strength for PEO with molecular weight of 20kDa. (From top to bottom, the lines successively represent the results of combinations with bottom thickness of 50nm, 12nm, 8.5nm, 5nm, 2.5nm).

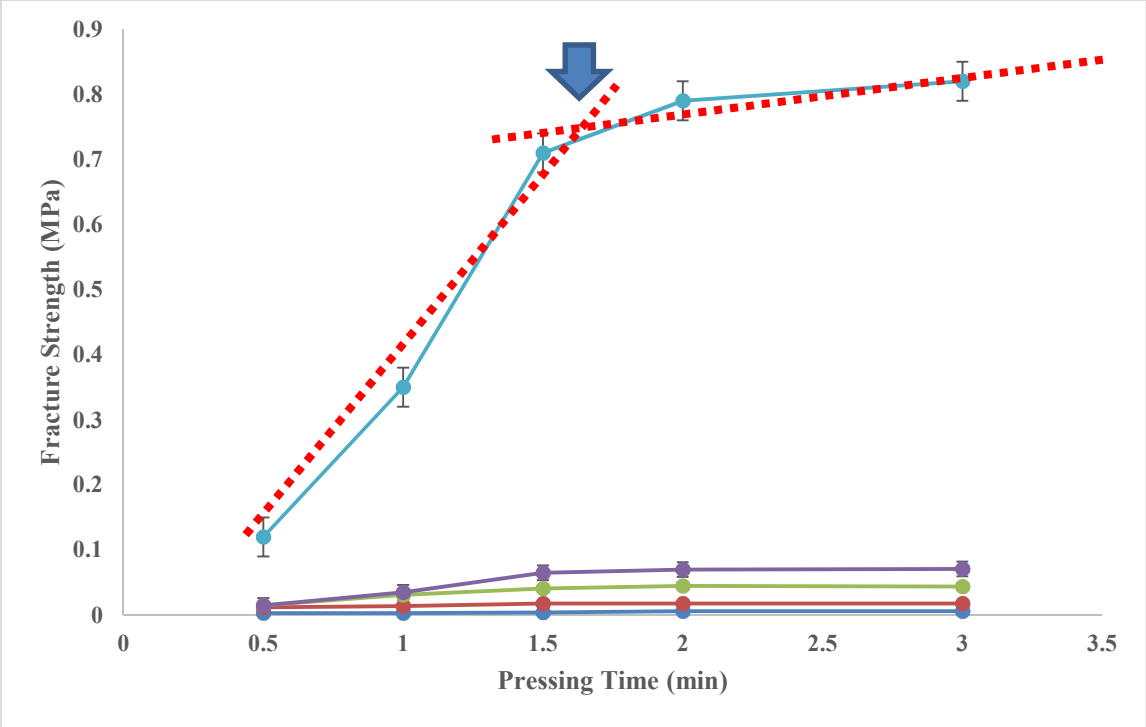

Figure 13. The pressing time dependence of the fracture strength for PEO with molecular weight of 20kDa. (From top to bottom, the lines successively represent the results of that combination with bottom thickness of 50nm, 12nm, 8.5nm, 5nm, 2.5nm).

From the figures, we can see that when pressing temperature is above the melting point of 65°C and pressing time is set longer than the reptation time for chain motion and entanglement, which is nearly 100s for PEO,[19] the fracture strength basically remain the same. The two critical points are indicated by the arrows in the figures.[20]

3.6 Thickness and molecular weight dependence of fracture strength

Fig. 14 shows the thickness and molecular weight dependence of the fracture strength of the bilayers composed of 8kDa, 20kDa and 100kDa. From the figure we can see that the fracture strength shows a parabolic relationship, which is in a good agreement with previous reports.[18,21] The phenomenon could be attributed to more sites for polymer chain entanglements due to the existence of thicker thin films.[22,23] This figure also indicates molecular weight dependence on fracture strength.[23] With higher molecular weight, the two attached polymer thin films are more difficult to be broken away from each other, since higher degree of polymerization increases the

number of polymer interaction sites. Hence, the interface could endure a larger force before it becomes crack.[24]

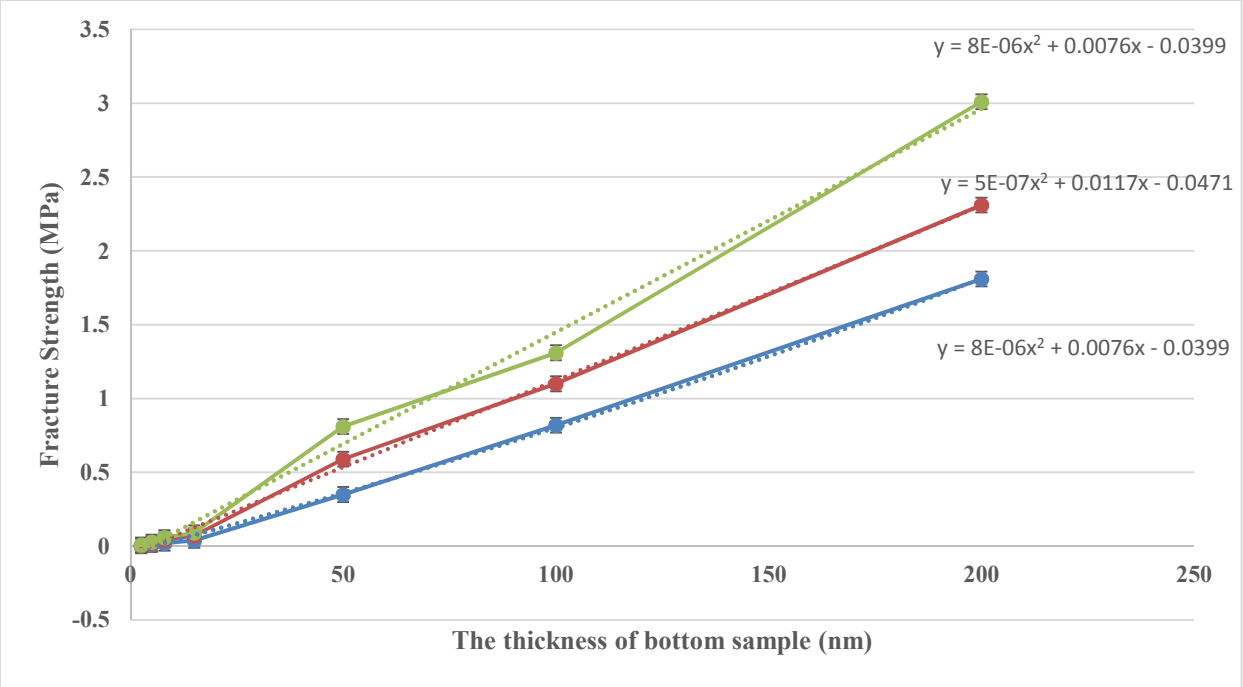

Figure 14. The thickness and molecular weight dependence of fracture strength. (From top to bottom, the lines successively represent the results of polymer with molecular weights of 100kDa, 20kDa and 8kDa).

The reasons for these two results could both regarded as a consequence of more polymer chain entanglements, while these different parameters will have effect at two locations, i.e., the interfacial region and the region of original polymer layer consisting of only one kind of polymer.

3.6 Chain conformation and structure dependence of fracture strength

As discussed above, the spin coated polymer thin film would have polymer chain adsorbed onto the silicon substrate via thermal annealing. The adsorbed nanolayer is composed of two distinguished layers, which could be uncovered by utilizing different leaching solvent with varying desorption energy, respectively.

In this section, I hence aimed to reveal the effects of the two adsorbed nanolayers on the fracture strength. Note that the thickness for all the upper samples was fixed to 200 nm. And as tabulated in Table 2, 3, 4 and 5, “A”, “B” and “C” represent different molecular weights: (A): 8kDa; (B): 20kDa; (C): 100kDa. The thickness of the flattened layer was 2.5 nm regardless of molecular weight, while the thicknesses of the interfacial sublayer were 5 nm for 8kDa, 8.5 nm for 20 kDa and 15nm for 100kDa, respectively..

Table 2. The fracture strength characterization of combinations with bottom thickness as 2.5nm for both spin coated thin film and adsorbed nanolayers.

Bottom sample	**2.5 nm thickness**		
Spin coated thin films	**A**	**B**	**C**
	0.004MPa	**0.006MPa**	**0.016MPa**
Adsorbed nanolayers (flattened layer)	**A**	**B**	**C**
	No Adhesion	**No Adhesion**	**No Adhesion**

Table 3. The fracture strength characterization of combinations with bottom thickness as 5nm for both spin coated thin film and adsorbed nanolayers.

Bottom sample	**5 nm thickness**		
Spin coated thin films	**A**	**B**	**C**
	0.009MPa	**0.018MPa**	**0.035MPa**
Adsorbed nanolayers (interfacial sublayer)	**A**	**B**	**C**
	0.01MPa	**0.019MPa**	**0.036MPa**

Table 4. The fracture strength characterization of combinations with bottom thickness as 8.5nm for both spin coated thin film and adsorbed nanolayers ("N/A" means that corresponding data is not available).

Bottom sample	**8.5 nm thickness**		
Spin coated thin films	**A**	**B**	**C**
	0.031MPa	**0.044MPa**	**0.092MPa**
Adsorbed nanolayers (interfacial sublayer)	**A**	**B**	**C**
	N/A	**0.044MPa**	**0.096MPa**

Table 5. The fracture strength characterization of combinations with bottom thickness as 15nm for both spin coated thin film and adsorbed nanolayers ("N/A" means that corresponding data is not available).

Bottom sample	**15 nm thickness**		
Spin coated thin films	**A**	**B**	**C**
	0.059MPa	**0.088MPa**	**0.145MPa**
Adsorbed nanolayers (interfacial sublayer)	**A**	**B**	**C**
	N/A	**N/A**	**0.145MPa**

The experimental results clearly show that the interfacial sublayer has similar adhesive force to that of the spin-cast films with the same film thicknesses, while the flattened layer always shows no adhesion. This difference may come from polymer chain entanglements: while the structure would provide no possibility for chain entanglements, the unique conformation of the interfacial sublayer provide sites for entanglement, resulting in stronger adhesion.[25]

3.7 Use of oligometer to study the effect of chain entanglements.

In order to further investigate the relationship between adhesion behavior and chain entanglement, PEO with molecular weight of 1.5kDa, which is smaller than the critical M_w of PEO for chain entanglement (M_c=1.84kDa[26]) was used. This polymer was purchased from Fluka Analytical.

We made a series of bilayers composed of an upper layer of 200 nm-thick and bottom spin coated thin film or the adsorbed nanolayers layer of 2.5 nm, 5 nm and 8.5 nm in thickness. The results are summarized in Table 6.

Table 6. The fracture strength characterization between polymers with higher molecular and polymer with lower molecular weight than critical value, with thickness and chain structure as controlled variables ("N/A" means that corresponding data is not available).

Bottom thickness	**Spin coated thin film**		**Adsorbed nanolayers**	
2.5 nm thickness	**1.5K**	**No Adhesion**	**1.5K (flattened layer)**	**No Adhesion**
	20K	**0.006MPa**	**20K (flattened layer)**	**No Adhesion**
	100K	**0.016MPa**	**100K (flattened layer)**	**No Adhesion**
5 nm thickness	**1.5K**	**No Adhesion**	**1.5K**	**N/A**
	20K	**0.018MPa**	**20K**	**0.019MPa**
	100K	**0.035MPa**	**100K**	**0.036MPa**
8.5 nm thickness	**1.5K**	**No Adhesion**	**1.5K**	**N/A**
	20K	**0.044MPa**	**20K**	**0.044MPa**
	100K	**0.096 MPa**	**100K**	**0.097 MPa**

As expected, no adhesive force was observed for the bilayers composed of the lowest M_w PEO (M_w=1.5kDa). Hence, it is reasonable to conclude that the null adhesion force of the flattened layer is due to the lack of chain entanglement.

3.9 Polymer bilayer dewetting experiments

Polymer thin film can either wet or dewet on an impenetrable solid surface. And whether the dewetting would take place or not depends on several factors including polymer-substrate interfacial energy, film thickness, polarity.[10] For this experiment, we focused on the interactions between polymer thin film and bottom substrate. And also, the bottom adsorbed nanolayers are considered as a "substrate". In case of wetting, a thin polymer film remains homogeneous and flat with a nearly zero contact angle with the substrate at equilibrium. Otherwise, the film would encounter a dewetting process from the initial rupture and growth of holes, coalescence into polygonal network, to the formation of dewetting droplets with clear three phase contact lines and a non-zero contact angle with regard to the solid substrate.

In this section, I prepared two bilayer samples by following the process shown below. After we prepared the PEO nanolayers on the HF-Si substrates, we spun coat another PEO thin film onto top.

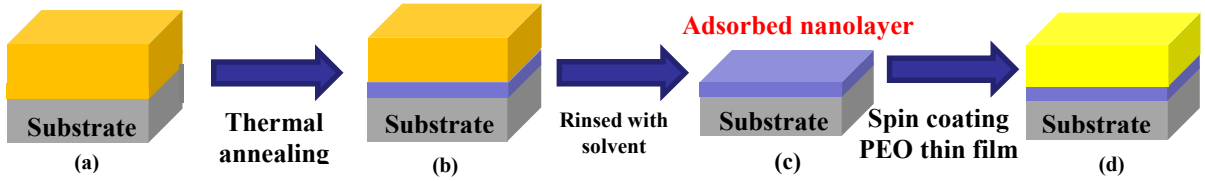

Scheme 4. Sample preparation process used in experiment

The first sample was PEO (M_n=20kDa) 50 nm thin film spin coated on the PEO (M_n=20kDa) interfacial sublayer, while the second sample was PEO (M_n=20kDa) 50 nm thin film spin coated on the PEO (M_n=20kDa) flattened layer. We annealed these samples to initiate the process of relaxing the residual stress and induce dewetting, if applicable. The AFM instrument was used to capture the surface morphology.

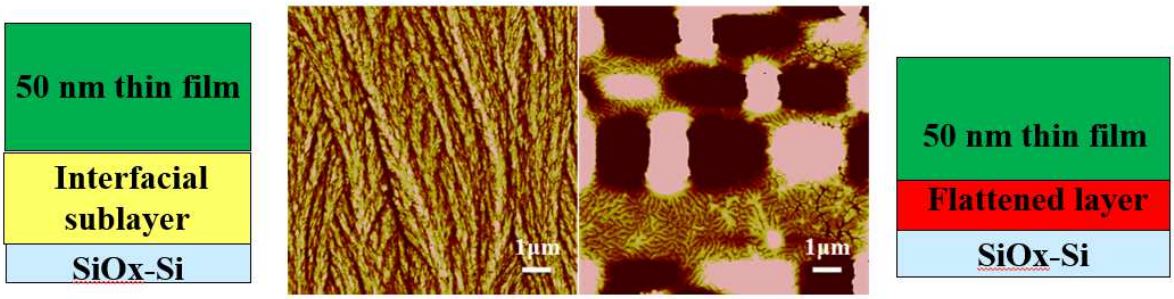

Figure 15. AFM images of the bilayer samples and the corresponding sample configurations.

As shown in Fig. 15, the AFM image (the left image) of the PEO thin film on the interfacial sublayer shows an edge-on crystalline morphology which can be seen in the bulk PEO film. On the other hand, the AFM image of the PEO thin film on the flattened layer showed a typical dewetting pattern. This phenomenon can be explained by the fact that the surface of the interfacial sublayer is wettable, while the surface of the flattened layer is slippery.[27] According to our previous neutron reflectivity experiment, it was found that a relatively wide interfacial width between the top thin film and the interfacial sublayer is developed compared to that between the top thin film and the flattened layer.[10] On the other hand, in the case of the flattened layer, its stable structure and insusceptible chain conformation prevent from interdiffusion between free chains and the flattened chains. This result is supportive for our theory: the different chain structures play a crucial role in the opposite adhesive properties.

3.10 Contact angle measurement and surface tension measurements

For this purpose, we used KSV CAM 200 optical contact angle meter to measure the static contact angle.[28] The volume of a droplet for each experiment was fixed as ~ 2 mL. The calculation of the surface tension was based on the two-component theory, i.e., the polar component and the dispersion component. Based on the young`s equation (eq. 3), fowkes theory equation (eq. 4), and reference parameters of the test liquids, which are tabulated in Table. 7, the two components could be calculated. The sum of these components then is equivalent to the entire surface tension. Note that during actual measurement process, the room temperature, the atmospheric pressure and so on have an impact on the experimental result.

$$\sigma_s = \sigma_{sl} + \sigma_l * \cos\theta \quad (3)$$

$$\sigma_{\mathrm{sl}} = \sigma_s + \sigma_l - 2*(\sqrt{\sigma_s^D * \sigma_l^D} + \sqrt{\sigma_s^P * \sigma_l^P}) \quad (4)$$

Table 7. The corresponding parameters of used test liquid at room temperature and atmospheric pressure

Chemical	Surface Tension (mN/m)	Dispersion Component (mN/m)	Polar Component (mN/m)
1, 4-butanediol	**44**	**24**	**20**
Glycerol	**64**	**34**	**30**

The static contact angle measurements using glycerol was measured and the results are shown in Fig. 16. We can see that despite of different chain structure or varying thickness, the static contact angle always remains unchanged (θ=44±1°). Even if some values of contact angle are deviated as the images indicate, they can still be considered as identical in the procedure of calculating surface tension since the trigonometric function will mitigate the negative effect due to practical experimental parameters to a level that it can be neglected.

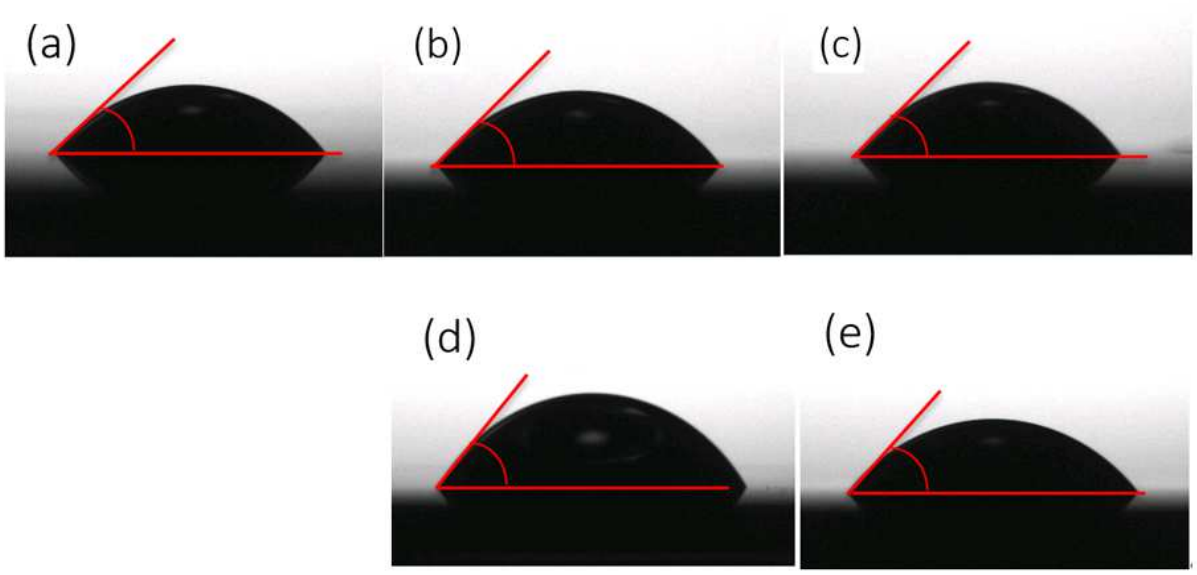

Figure 16. The static contact angle of PEO with molecular weight as 20kDa using glycerol as test liquid: (a) 50nm spin coated thin film (b) 8.5nm interfacial sublayer (c) 2.5nm inner flattened layer (d) 8.5nm spin coated thin film (e) 2.5nm spin coated thin film.

In order to gain the accurate value of the surface tension, we continued the experiments by utilizing a second test liquid: 1, 4-butanediol. Water is typically used as a test liquid, but is not appropriate for PEO since it is soluble in water. The static contact angle using this liquid is measured as around 13±4°. The contact angle data using 1, 4-butanediol is shown in Figure 17.

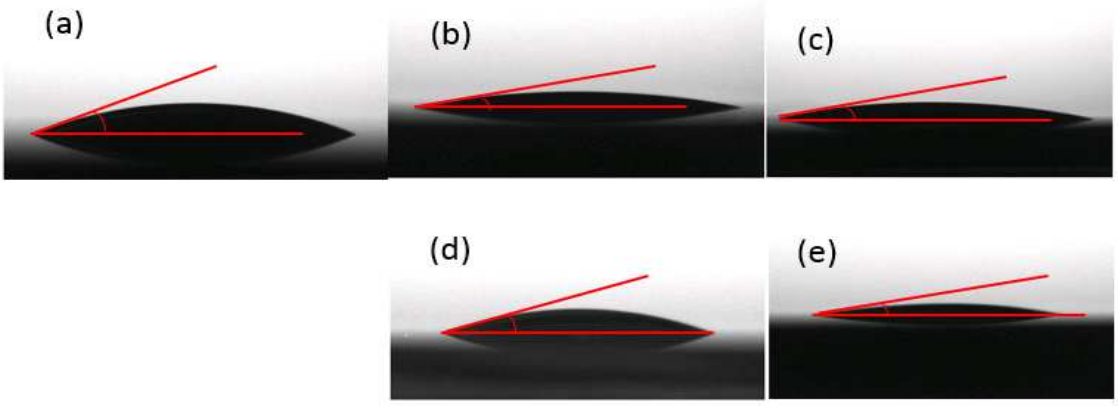

Figure 17. The static contact angle of PEO with molecular weight as 20KDa using 1,4-butanediol as test liquid: (a) 50nm spin coated thin film (b) 8.5nm interfacial sublayer (c) 2.5nm inner flattened layer (d) 8.5nm spin coated thin film (e) 2.5nm spin coated thin film.

With the data above, the surface tension of the PEO film was determined as follows: the dispersion component as 30.25mN/m and polar component as 14.45mN/m, and the surface tension as 44.7mN/m regardless of its thickness and chain structures. The surface tension data is in a good agreement with previous data.[29] For an interface between two identical materials, it is expected from eq. (1) that the thermodynamic work of adhesion is simply twice the surface tension; $W_{AB}=2\sigma_{A.}$ However, as evidenced by our experimental data, the final fracture strengths between the spin cast film and flattened layer are different. Hence, additional factor associated with chain entanglements crossed the interface need to be considered to explain the experimental results.[2,30] Further experiments deserve future work.

Chapter 4. Conclusion

After thermal annealing and subsequent appropriate solvent leaching, different adsorbed nanolayers with different chain structures and surface morphologies can be derived from spin cast polymer thin films. From the discussion above, our results indicate that the homopolymer interfacial sublayer could show a consistently similar adhesive behavior to spin cast thin fim, with characterized by fracture strength, while the flattened layer manifests the completely opposite property, i.e. totally no adhesion. Hence, we propose the following hypothesis to explain this phenomenon based on their nanoscale chain structures: the interfacial sublayer with the relatively loose chain structure and fewer attaching points to a substrate would be more easily mobile and thus create chain entanglement with free polymer chains at the top overlayer. On the other hand, the flattened layer possesses more attaching points to the substrate and more unsusceptible chain structure that is sufficiently enough to keep it stable and prevent from any entanglements or interactions between itself and the top thin film. In order to further substantiate our hypothesis, we conduct two relative experiments, i.e. the dewetting experiment and the fracture strength characterization using polymer of quite low molecular weight, and both of them help prove the reasonability of our hypothesis. Additionally, static contact angle measurements indicate that the same surface tension for polymer films regardless of their thickness and structure. Furthermore, two dimensional GID patterns demonstrate that the melting point of interfacial sublayer is bulk-like.

References

[1] A.C.N. Singleton, C.A. Baillie, P.W.R. Beaumont, T. Peijs, Composites: Part B **34**, 519 (2003).

[2] S. J. Bennett, K. L. Devries and M. L. Williams, International Journal of Fracture **10** (1), 33 (1974).

[3] K.L.MITTAL, Electrocoponent Science and Technology **3**, pp. 21 (1976).

[4] Stefano Burattini, Barnaby W. Greenland, David Chappell, Howard M. Colquhoun and Wayne Hayes, Chemical Society Reviews **39**, 1973 (2010).

[5] Phillip J. Cole, Robert F. Cook, and Christopher W. Macosko, Macromolecules **36** (8), 2808 (2003).

[6] Ralf Schnell and Manfred Stamm, Macromolecules **32** (3420-3425) (1999).

[7] N.K. Myshkin, M.I. Petrokovets, A.V. Kovalev, Tribology International **38**, 910 (2005).

[8] Mark J. Stevens, Macromolecules **34**, 2710 (2001).

[9] A.A. Volinsky, N.R. Moody, W.W. Gerberich, Acta Materialia **50**, 441 (2002).

[10] Naisheng Jiang, Jun Shang, Xiaoyu Di, Maya K. Endoh, and Tadanori Koga, Macromolecules **47** (8), 2682 (2014).

[11] Peter Gin, Naisheng Jiang, Chen Liang, Takashi Taniguchi, Bulent Akgun, Sushil K. Satija, Maya K. Endoh, and Tadanori Koga, Physical Review Letters **109** (26), 265501 (2012).

[12] Mitsunori Asada, Naisheng Jiang, Levent Sendogdular, Jonathan Sokolov, Maya K. Endoh, Tadanori Koga, Masafumi Fukuto, Lin Yang, Bulent Akgun, Michael Dimitriou and Sushil Satija, Soft Matter **10**, 6392 (2014).

[13] H. Ade, D. A. Winesett, A. P. Smith, S Anders, T. Stammler, C Heske, D. Slep, M. H. Rafailovich, J. Sokolov, J. Stohr, Applied Physics Letters **73** (25), 3775 (1998).

[14] Julia Nase, Oscanny Ramos, Costantino Creton, and Anke Lindner, The European Physical Journal E **36** (9), 1 (2013).

[15] William W. Merrill and Alphonsus V. Pocius, Langmuir **7**, 1975 (1991).

[16] Chelsea S. Davis, Florian Lemoine, Thierry Darnige, David Martina, Costantino Creton, and Anke Lindner, Langmuir **30**, 10626 (2014).

[17] David Arencon and Jose Ignacio Velasco, Materials **2**, 2046 (2009).

[18] J. E. Ritter, T. J. Lardner, L. Rosenfeld, and M. R. Lim, Journal of Applied Physics **66** (8), 3626 (1989).

[19] Nikolaos A. Peppas and J. C. Wu, Macromolecules **27**, 5626 (1994).

[20] A. N. Gent, Langmuir **12**, 4492 (1996).

[21] H. R. Brown, Annual Reviews Material Science **21**, 463 (1991).

[22] T. Kerle, J. Klein, and K. Binder, The European Physical Journal B **7**, 401 (1999).

[23] Ralf Schnell and Manfred Stamm, Macromolecules **31**, 2284 (1998).

[24] Firas Awaja, Michael Gelbert, Georgina Kelly, Bronwyn Fox, Paul J. Pigram, Progress in Polymer Science **34**, 946 (2009).

[25] Andrew V. Zhuk, Anthony G. Evans, and John W. Hutchinson, George M. Whitesides, Journal of Materials Research **13** (12), 3555 (1998).

[26] L. J. Fetters, D. J. Lohse and R. H. Colby, in *Physical Properties of Polymers Handbook*, edited by James E. Mark (Springer-Verlag New York, United States, 2006), pp. 445.

[27] Gunter Reiter and Rajesh Khanna, Langmuir **16**, 6351 (2000).

[28] D. Y. Kwok, A. W. Neumann, Advanced in Colloid and Interface Science **81**, 167 (1999).

[29] C. J. van Oss, M. K. Chaudhury, and R. J. Good, Advanced Colloid Interface Science **28**, 35 (1987).
[30] Souheng Wu, The Journal of Adhesion **5** (1), 39 (1973).